Digital Object Identifier: 10.1109/ULTSYM.2008.0263

Acoustic Characterisation of Individual Targeted Microbubbles with High-Frequency Ultrasound

Michael R. Sprague, David E. Goertz, Emmanuel Chérin, Raffi Karshafian, F. Stuart Foster
Department of Medical Biophysics, Sunnybrook Research Institute
University of Toronto, Canada
michael.sprague@sri.utoronto.ca

***Abstract* — The acoustic response of individual targeted microbubbles, sized optically, to high-frequency ultrasound was examined to improve nonlinear imaging techniques and aid signal quantification. Single bound phospholipid shell microbubbles (diameters 1.0 to 5.0 µm) were insonated with 30 MHz Gaussian-shaped pulses for pressures from 20 kPa to 4 MPa with a fractional -6dB one-way bandwidth of 20%. The scattering cross-section, subharmonic and second harmonic SNR, and microbubble disruption (determined acoustically and verified optically) was measured. The effective scattering cross-section was found to be, on average, 2 times lower than the geometric cross-section; showing size-independent variability. The subharmonic signal increased above the noise floor at 150 kPa, showing a clear peak around 1.5 µm; the behaviour at pressures above 400 kPa was more complex. The second harmonic SNR appeared to arise predominately from the presence of nonlinear propagation. The disruption threshold was size-dependent, 400 ± 200 kPa for microbubbles less than 1.5 µm in diameter and over 2 MPa for microbubbles larger than 2.5 µm.**

Keywords- High-frequency ultrasound; targeted microbubbles; subharmonic; molecular imaging

I. INTRODUCTION

Assessing anti-angiogenic therapies and detecting incipient cancers may benefit from imaging the molecular pathways responsible for tumour growth. [1] Receptor tyrosine kinases and integrins on endothelial cells are components of the angiogenic cascade that lead to tumour permeability, migration and vessel growth. [2] Non-invasive imaging of endothelial markers is possible with the detection of targeted microbubbles. [3,4]

Microbubbles are effective ultrasound contrast agents (with scattering cross-sections orders of magnitude larger than their geometric cross-section at resonance [5]) that can bind to intravascular receptors through conjugated antibodies or small peptides. Microbubble coupling to a time varying pressure field is inherently nonlinear, generating higher harmonics from asymmetric oscillations. Microbubbles oscillating near surfaces have a modified resonant frequency [5] and increased damping [6]. Lastly for certain parameters (pressure, radius, frequency, shell properties) subharmonic oscillations (f_0/N, N=2,3… (herein N=2)) and other heterodyne frequencies can be generated. [7]

High-frequency ultrasound (20-40 MHz), with higher resolution and attenuation, has applications in small-animal [8] and intravascular imaging. Nonlinear emissions from diagnostic microbubbles have been observed at higher frequencies. [9] Particularly relevant to imaging is the subharmonic emission, which is not corrupted by tissue harmonics. *In vitro* and *in vivo* studies have demonstrated the feasibility of subharmonic imaging. [10] The exact cause of the subharmonic emission is not well understood, though the shell elastic behaviour is thought to be important. [11,12] Intriguingly, the shell properties appear to be frequency dependent, with a shell viscosity an order of a magnitude lower at high-frequencies compared to diagnostic frequencies. [13] Second harmonic (20 MHz transmit) and subharmonic (30,40 MHz transmit) imaging of microbubble populations (1-2 µm dia. and below) has been demonstrated for free flowing [14] and bound [15] conditions.

Direct knowledge of the size dependence of nonlinear scattering at high frequencies is lacking, as is insight into the influence of a boundary on nonlinear generation. This motivates a study to examine the size-dependent behaviour of single microbubbles at high frequencies. Specifically, the scattering cross-section, subharmonic and second harmonic generation and disruption threshold will be measured. The application of this work is to optimise the parameters for nonlinear high-frequency imaging of targeted microbubbles for translation to *in vivo* studies.

II. METHODS

Single targeted phospholipid shell microbubbles (diameters 1.0 to 5 µm) were insonated with 30 MHz Gaussian-shaped pulses for pressures from 20 kPa to 4 MPa with a fractional -6 dB one-way bandwidth of 20% (at 220 kPa).

A. Sample Preparation

Micromarker™ targeted microbubbles [1] (Visualsonics), prepared to manufacturer's specifications and diluted 7500 to 30000 times by volume with a degassed phosphate buffered solution were deposited on a thin layer of 3% by weight gelatin and then washed with distilled, degassed water.

[1] Mean volume weighted diameter 4 µm, full width at half maximum 4 µm, phospholipid monolayer shell with embedded streptavidin and nitrogen/ perfluorobutane gas core) (Visualsonics)

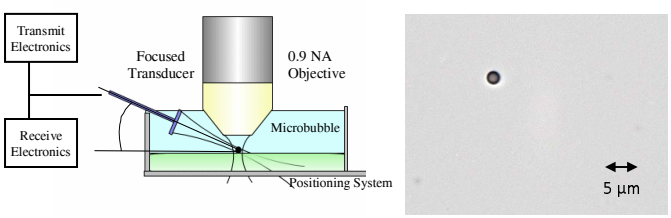

Figure 1. *Schematic of experimental setup and optical image (2.2 µm dia.)*

B. Alignment

The sample was mounted on a precision positioning system (Aerotech HDZ1M) and aligned under an upright microscope and single element transducer. (see figure 1) Individual glass beads (75 µm dia.), manipulated by a micropipette, facilitated optical and acoustic alignment. The transducer (on independent positioning system (Newport)) was at an angle of 69 degrees from normal incidence to the sample, calculated to minimize off-axis interference caused by the objective (the pressure was 25 dB below the on axis pressure at the closest point to the objective).

C. Optical Setup

Microbubbles were sized with a 2.2 mm free-working distance, 0.9 NA water-immersion objective and 0.9 NA condenser at 4-5 mm. Images were digitized by a camera (Leica DFC300) with a pixel size of 0.10 µm under magnification. The system resolution was characterised by the modulation transfer function of parallel slits using a test slide (Richardson); showing a spatial modulation of 0.5 at 0.8 µm and 0.1 at 0.5 µm. Image analysis was performed offline with MATLAB. To size the microbubbles a region-of-interest was chosen around the bubble; a pixel intensity half way between the median intensity (representing the background) and the minimum intensity was used as a threshold. [16] The filled, segmented image's pixel area was used to estimate the microbubble's diameter. A random, size-dependent error due to variance in the focal plane sampled was calculated to be 5% for microbubbles less than 1.5 µm, and 2% for microbubbles between 3-4 µm. There may also be a systematic error due to complex light scattering phenomenon.

D. Acoustic Pulses

The transducer employed was a 25 MHz 100% - 6dB two-way fractional bandwidth f# 2.1, focal length = 15 mm single element spherically focused transducer driven at 30 MHz. The pulses were generated by an arbitrary wave generator (Tektronix AWG2021) and amplified by a gated 60 dB pulse amplifier (AMT M3205, 6-220 MHz). At each pressure 32 pulses were sent with a PRF of 1 kHz, with 1 second between pressures to observe size changes. Seventeen pulse pressures were sent with peak negative pressures (PNP) of 20 kPa to 4.2 MPa, characterized by a calibrated 40 µm needle hydrophone (Precision Acoustics). Optical images were taken before and after each set of sequences. The scattered pressure waves were received, amplified by a 47dB amplifier (MITEQ AU1313 5-500MHz) and digitized by an 8-bit ADC (Acqiris DO240) at 500 MHz. The receive acquisition settings were kept constant, though a 10dB attenuator was placed before the pre-amplifier for pressures from 1 to 4 MPa (noise floor unchanged). Noise only acquisitions were performed at the same settings, with the AWG transmit off. A 250 point tapered cosine window (taper ratio 0.5) was applied symmetrically about the focus. When comparing energy in the different frequency bands, the fundamental was integrated over the -6dB two-way bandwidth; the subharmonic and second harmonic were integrated over a 5 MHz bandwidth centered at 15 MHz and 60 MHz, respectively (noise subtracted). For the subharmonic signal to noise ratio (SNR) means and standard deviations were calculated in the linear domain, and have not been corrected for attenuation or the transducer's bandwidth.

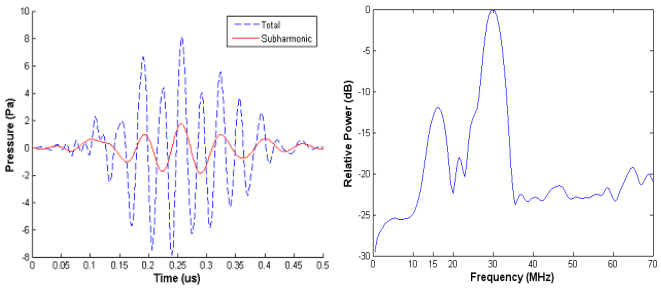

Figure 2. *Time domain signal from 1.5 µm dia. microbubble for transmit 220 kPa, spectrum, showing clear subharmonic (32 pulses averaged).*

E. Scattering Cross-section

To characterise the effectiveness of microbubbles for imaging, the scattering cross-section, or effective scattering cross-section is useful. The scattering cross-section is the area of a perfectly reflecting particle that scatters the same amount of energy as the object, defined as:

$$\sigma = \lim_{r\to\infty} 4\pi r^2 \frac{\langle p_{sc}^2 \rangle}{\langle p_{inc}^2 \rangle} \qquad (1)$$

Where r is the distance from the microbubble and $\langle p^2 \rangle$ is the time average of the pressure squared. The scattering cross-section is defined over all frequencies. Experimentally, attenuation [17] and the bandwidth of the transducer require an effective cross-section to be defined.

$$\sigma_{eff} = \frac{4\cdot\pi\int_{-\infty}^{\infty} r^2 |p_{sc}(f)|^2 \cdot e^{-\alpha(f)\cdot r} BW(f)df}{\int_{-\infty}^{\infty} |p_{inc}(f)|^2 \cdot e^{-\alpha(f)\cdot r} BW(f)df} \qquad (2)$$

Where α is the frequency dependent attenuation (e.g. in water) and BW the bandwidth (the received echo is convolved with these two). In general, the scattering cross-section will have an angular dependence, as the scattering of a bound microbubble may not be isotropic [18]. To determine the scattered pressure the receive transfer function must be calibrated. This was done by calibrating the response reflected by a quartz block to the pressure measured by a hydrophone at twice the focal distance and integrated over the area of the transducer. (Details forthcoming)

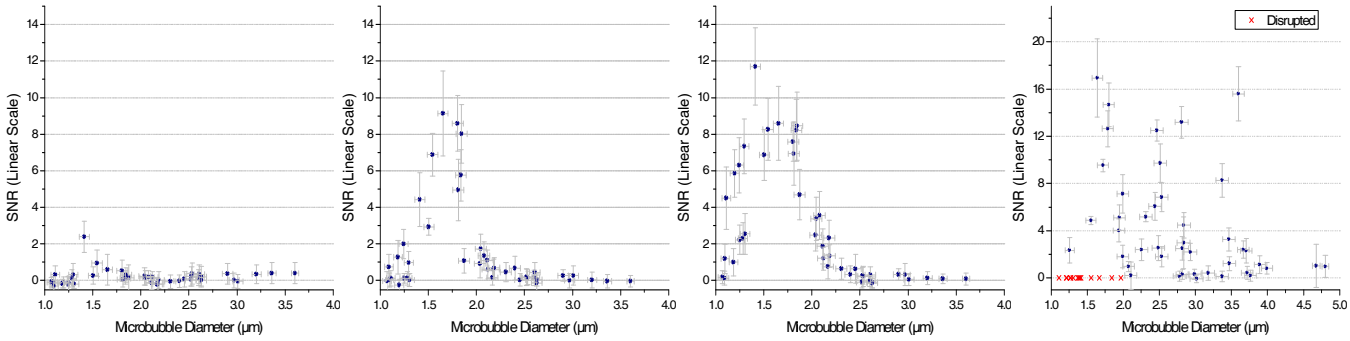

Figure 3. *Subharmonic SNR for 110, 150, 200, and 810 kPa PNP (±10%) (N=46), Error bars are standard deviations (N_y=32)*

III. Results

A. Representative Analysis

Figure 2 shows a representative series of measurements. A single microbubbles was imaged (figure 1), a sequence of 32 pulses with a PNP of 220 kPa was transmitted and averaged, the received echo, filtered for noise (6^{th} order low pass Butterworth filter f_c = 75 MHz) is shown (figure 2). The subharmonic component was filtered (non-causal (zero-phase distortion) 12^{th} order Butterworth f_c = 20 MHz). Note the relative phase between the fundamental and subharmonic signal ensures the positive pressure is modulated. The spectrum shows a clear subharmonic component. Note the lack of second harmonic above the noise floor.

B. Subharmonic Signal

The subharmonic SNR was calculated for each microbubble at each pressure. Forty-six microbubbles were subjected to 7 sets of pulses (20% bandwidth) with pressures from 20 kPa to 200 kPa. Fifty-eight separate microbubbles were interrogated with 7 sets of pulses from 220 kPa to 1 MPa for the same bandwidth. Microbubble responses at fixed pressures are shown on Figure 3. The results were regridded, shown in figure 4, with no *a priori* assumption of parametric spatial correlation of bubble responses (triangulation with c1 cubic spline interpolation (smoothing = 0.006)). Ultraharmonic energy ($3f_0/2$) was rarely observed above the noise floor, except in conjunction with broad-band emissions.

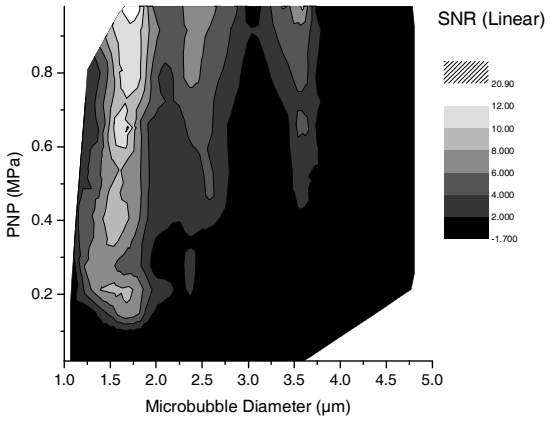

Figure 4. *Subharmonic SNR for 20% bandwidth pulse as a function of microbubble diameter (N=58) and pressure (N=14).*

C. Second Harmonic Signal

At 60 MHz the transducer sensitivity was -21 dB lower than the centre frequency. The second harmonic signal increased above the noise floor at approximately 380 kPa and its power scales proportional to the pulse power squared for microbubbles not undergoing disruption. The signal also scaled with the physical cross-section, as expected for linear scattering of nonlinear energy. Additionally, linear scatterers showed a similar behaviour, suggesting the detected second harmonic is predominately caused by nonlinear propagation of the high-frequency ultrasound wave, and not a result of harmonic generation from the microbubble. (Data not shown)

D. Scattering Cross-section

The results, measured with a 220 kPa pulse, is shown in figure 5, and the scattering cross-section predicted for a free-gas bubble (equal to its *geometric* cross-section) is shown for comparison. In general, the scattering cross-section showed pressure dependence as well. (Details forthcoming)

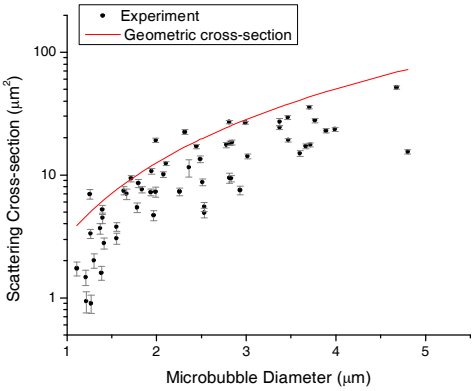

Figure 5. *Effective scattering cross-section, 220 kPa, 20% bandwidth. The geometric cross-section is equal to the scattering cross-section of a free gas bubble (N=58, error bar = std. dev (N_2=32).)*

E. 'Disruption' Threshold

The acoustic signal from microbubbles decreased with increasing pulse power in certain instances, defined herein as the 'disruption' threshold. This behaviour was correlated optically with a decreasing physical size. The threshold for a 20% bandwidth pulse is shown in figure 6. The threshold was dependent on the number of pulses sent, and the length of the pulse (the threshold shifted higher for the shorter bandwidths).

Control experiments demonstrated microbubble stability during the measurments. Sending lower pressure pulses did not influence the higher pressure response of the microbubble until the disruption threshold was reached (i.e. no hysteresis).

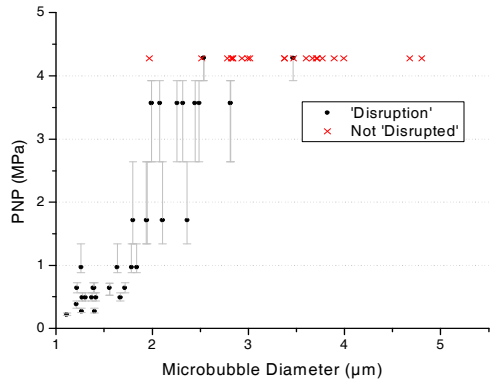

Figure 6. *Disruption threshold for 20% bandwidth pulses (N=58)Not 'disrupted' are microbubbles that remained stable through the experiment*

IV. Discussion

The binding method is non-specific; the gelatin does not contain biotin. However, the binding was reproducible and stable; any difference between biotin-streptavidin binding and non-specific binding is assumed to be a second-order effect, or lower. Additionally, no comparison between free and bound microbubbles was attempted; these results may not extend to free-flowing microbubbles.

The mechanism of disruption is not entirely clear, though a fast-frame camera (on the order of the PRF) may be instructive. Briefly, microbubbles smaller than approximately 1.75 µm 'disrupt' below 1 MPa, progressively shrinking until disappearing or becoming detached from the surface. The fundamental frequency signal decayed, without the broad-band acoustic signal characteristic of cavitation. Above 1 MPa, microbubbles (>1.75 µm) either remained or became disrupted; shrinking and often displaying a broad-band signal with strong subharmonic ($f_0/2$) and ultraharmonic ($3f_0/2$) signals, which may be from small gas bubbles separating from the microbubble and oscillating aperiodically.

The scattering cross-sections calculated in figure 5 demonstrate two important points. One, there is size-independent variability, which may represent variations in binding or shell properties. Two, the scattering cross-section is approximately 2 times lower than the microbubble's geometric cross-section, implying a damping coefficient on the order of 1 assuming the microbubbles are far from their resonant frequency.

The subharmonic signal increased above the noise floor at 150 kPa, displaying a clear threshold, with a peak around 1.5 µm for pressures up to 400 kPa. A 1.5 µm diameter microbubbles has an eigenfrequency of 15 MHz (minimum frequency to excite subharmonic) for a shell elastic modulus of 0.9 N/m, comparable to the elastic modulus of Definity microbubbles (lipid coated octafluoropropane) at high-frequencies (0.8-0.85 N/m). [13] Above 400 kPa, microbubbles below 1.7 µm become disrupted, while larger microbubbles emit subharmonic energy. The threshold and saturation of the subharmonic signal has been previously noted for low [19] and high frequencies [14], although these results appear to be the lowest threshold measured. The relative phase of the subharmonic signal ensured modulation of the expansion of the microbubble, this was observed for all microbubbles except those exhibiting a broad-band signal above 1 MPa. Overall, a complex parameter structure is suggested for subharmonic emissions; more complete understanding of the mechanism responsible for subharmonic generation may provide further insight.

Acknowledgment

This work was supported by CIHR, ORDCF and the Terry Fox Program

References

[1] Ferrara N and Kerbel RS. *Nature* 2005:438;967
[2] Risau W. Mechanisms of Angiogenesis. *Nature* 1997: 386;671-674
[3] Klibanov AL. Ultrasound molecular imaging with targeted microbubble contrast agents. *J Nucl Cardiol* 2007;14:876-84
[4] Rychak JJ, Graba J et al. Microultrasound molecular imaging of vascular endothelial growth factor receptor 2 in a mouse model of tumor angiogenesis. *Mol Imaging* 2007;6,6:289-296
[5] Leighton TG. The Acoustic Bubble London: Academic Press, 1994
[6] Garbin V, Cojoc, C et al. Changes in microbubble dynamics near a boundary revealed by combined optical micromanipulation and high-speed imaging. *Appl Phys Lett* 2007;90
[7] Paulitz U, English V, et al. Bifurcation structure of bubble oscillators. . *Acou. Soc. Am* 1990;88:1061-1077
[8] Foster FS, Pavlin CJ et al. Advances in ultrasound biomicroscopy. *Ultrasound Med. Biol* 2000;26:1-27
[9] Goertz DE, Wong SWS et al. Nonlinear scattering properties of microbubble contrast agents at high frequencies. *Proc. IEEE Ultrason. Symp*. 2001:1747–1750.
[10] Goertz DE, Frijlink ME, et al. Subharmonic contrast intravascular ultrasound for *vasa vasorum* imaging. *Ultrasound Med Biol.* 2007;33:1859–1872
[11] Chatterjee D, Sarkar S et al. A Newtonian rheological model for the interface of microbubble contrast agents. *Ultrasound Med Biol* 2003;29:1749–1757
[12] Goertz DE de Jong N., van der Steen, AFW. Modeling high frequency nonlinear scattering from lipid encapsulated microbubble contrast agents. *Proc. IEEE Ultrason Symp*. 2007
[13] Goertz DE de Jong N, van Steen AFW. Attenuation and size distribution measurements of Definity™ and manipulated Definity™ Populations. *Ultrasound Med Biol* 2007;33:1376-1388
[14] Goertz DE, Frijlink ME et al. Nonlinear Intravascular Ultrasound Contrast Imaging. *Ultrasound Med Biol.* 2006;32:491–502
[15] Goertz DE, van Wamel A, et al. Nonlinear Imaging of Targeted Microbubbles with Intravascular Ultrasound. *Proc. IEEE Ultrason. Symp*. 2005.
[16] Postema M, Bouakaz A, et al. Simulation and measurements of optical images of insonified ultrasound contrast microbubbles. *IEEE Trans Ultrason Ferroelec Freq Control*. 50;523-535
[17] Hilgenfeldt S, Lohse D, Zomack M. Sound scattering and localized heat deposition of pulse-driven microbubbles. *J Acoust Soc Am* 2000;107:3530-3539
[18] Zhao S, et al. Asymmetric oscillation of adherent targeted ultrasound contrast agents. *Appl Phys Lett* 2005;87:134103
[19] Forsberg F, Shi WT, Goldberg BB. Subharmonic imaging of contrast agents. *Ultrasonics* 2000;38:93-98